

RESEARCH ARTICLE

10.1029/2018JA025660

Key Points:

- The small flux ropes have been categorized into four types considering the characteristics of the iron charge states
- Small flux ropes may have their twisted structures formed predominately during their eruption processes
- Small flux ropes are reconfirmed to have two source regions

Correspondence to:

J. Huang,
jhuang@swl.ac.cn

Citation:

Huang, J., Liu, Y. C.-M., Peng, J., Qi, Z., Li, H., Klecker, B., et al. (2018). The distributions of iron average charge states in small flux ropes in interplanetary space: Clues to their twisted structures. *Journal of Geophysical Research: Space Physics*, 123, 7167–7180. <https://doi.org/10.1029/2018JA025660>







Received 9 MAY 2018

Accepted 25 JUL 2018

Accepted article online 9 AUG 2018

Published online 8 SEP 2018

The Distributions of Iron Average Charge States in Small Flux Ropes in Interplanetary Space: Clues to Their Twisted Structures

Jia Huang¹ , Yong C.-M. Liu¹ , Jun Peng^{1,2} , Zhaohui Qi^{1,2}, Hui Li¹ , Berndt Klecker³ , Hongqiang Song⁴, Jinlei Zheng⁵, and Qiang Hu⁵ 
¹State Key Laboratory of Space Weather, National Space Science Center, Chinese Academy of Sciences, Beijing, China,

²College of Earth Sciences, University of Chinese Academy of Sciences, Beijing, China, ³Max-Planck-Institut für Extraterrestrische Physik, Garching, Germany, ⁴Institute of Space Sciences, Shandong University, Weihai, China,

⁵Department of Space Science and CSPAR, University of Alabama in Huntsville, Huntsville, AL, USA

Abstract Small flux ropes (SFRs) have been studied for decades, but their source regions and formation mechanisms are still under debate. In this study, we focus on the formation mechanism of the twisted structures of SFRs. Current research on magnetic clouds suggests five-type distributions of the time structure of iron average charge states ($Q_{\langle Fe \rangle}$), which imply different formation mechanisms of twisted structures. We use a similar method to identify the $Q_{\langle Fe \rangle}$ types of 25 SFRs. However, only four of these five types of distributions are found among these SFRs. Because different origins of SFRs are characteristically affecting the formation of $Q_{\langle Fe \rangle}$ types, the possible source regions of these SFRs are distinguished. With additional compositional parameters, SFRs are reconfirmed to originate from two types of source regions: the solar corona and the interplanetary medium. Based on these results, our analysis indicates that the twisted structures of SFRs originating from the solar corona may be formed predominately during eruptions. SFRs originating from interplanetary space are related to complex magnetic reconnection processes, which may result in intricate $Q_{\langle Fe \rangle}$ distributions due to the reconstruction of magnetic field topology.

1. Introduction

Magnetic flux ropes, associated with fundamental processes in space plasmas, are twisted magnetic field structures (e.g., Forbes, 2000; Gold & Hoyle, 1960; Linton & Moldwin, 2009; Tian et al., 2010; Wang, Zhuang, et al., 2016). In general, the sizes of magnetic flux ropes have continuous distributions from small scale to large scale (Feng et al., 2007). Large-scale flux ropes or magnetic clouds (MCs), which are considered to be a subset of interplanetary coronal mass ejections (ICMEs), usually have a timescale of 1 day (e.g., Burlaga et al., 1981; Jian et al., 2006; Shen et al., 2017; Tian et al., 2010). However, small-scale flux ropes (SFRs), which have been first reported by Moldwin et al. (1995, 2000), primarily have a limited duration of no more than 12 hr (e.g., Cartwright & Moldwin, 2008; Feng et al., 2015). Similar to large-scale MCs, SFRs can also be well fitted with the Lundquist flux rope model (Lundquist, 1950). Zheng and Hu (2018) also applied the Grad-Shafranov reconstruction technique (Q. Hu & Sonnerup, 2001, 2002) to identify SFRs. MCs are of great interest due to their associations with strong solar eruptions and potentially immense geoeffectiveness (e.g., H. Hu et al., 2016; Wang, Zhang, et al., 2016). SFRs contribute mainly to slow solar wind, and their source regions and formation mechanisms are still under discussion (e.g., Feng et al., 2007, 2015; Janvier et al., 2014a, 2014b; Kilpua et al., 2009; Tian et al., 2010; Yu et al., 2016, 2014; Zheng & Hu, 2018).

Different from MCs that originate from the solar corona, SFRs are believed to have two source regions: the solar corona and the interplanetary medium (e.g., Cartwright & Moldwin, 2008; Feng et al., 2015; Janvier et al., 2014b; Moldwin et al., 2000; Rouillard et al., 2009; Tian et al., 2010; Yu et al., 2016, 2014). SFRs originating in the solar corona can be classified into two categories. One category comes from the so-called *plasma blobs*, which are observed as twisted structures in the imaging observations (Sheeley Jr. et al., 2009; Song et al., 2009), that are released from the cusp of the streamer belt (Wang et al., 2000). Rouillard et al. (2009, 2011) confirmed this result by tracing several SFRs back to their source regions. But whether they are released through interchange reconnection processes (Huang et al., 2017; Wang et al., 2000) or pinched off by the intrinsic instability-driven magnetic reconnection processes (Chen et al., 1936) still needs further investigation. The other category may

be related to X-ray jets that arise from the photosphere (Janvier et al., 2014b). The widespread small magnetic loops that are rooted in the photosphere could, by interchange reconnection with adjacent open magnetic field lines, produce blowout jets, propagating into the solar corona and then into the heliosphere (Mandrini et al., 2005; Moore et al., 2010, 2013). Both observations and simulations indicate the helical structures of these jets (C. Liu et al., 2011; Moore et al., 2013). Furthermore, small-scale jets from the networks of the chromosphere and solar transition region (De Pontieu et al., 2014; Tian et al., 2014) may also contribute. In the interplanetary medium, SFRs could be formed from the heliospheric current sheet (HCS; Moldwin et al., 2000) or by the erosion of MCs (Feng & Wu, 2009). Moldwin et al. (1995) first suggested that multiple magnetic reconnection within HCS may help to develop a SFR. Feng et al. (2015) further found that SFRs can be divided into two categories according to whether they are in the vicinity of HCSs, implying the HCS should be one source of them. However, the thickness of HCSs is only about 10^4 km (Huang, Liu, Klecker, & Chen, 2016; E. Smith, 2001), which is about 10 times smaller than the smallest SFRs detected (Janvier et al., 2014b), provoking debate on such a formation mechanism. In addition, the magnetic flux of large-scale MCs could be partly eroded away by magnetic reconnection during its propagation (Mao et al., 2017; Ruffenach et al., 2012). The magnetic reconnection exhaust (Gosling et al., 2005; He et al., 2018; Mistry et al., 2017) at the boundary of a SFR could be a signature that links the erosion of MC to the formation of a SFR (Feng & Wu, 2009; Tian et al., 2010).

The twisted structures of both solar and interplanetary magnetic flux ropes have been studied in detail (Wang, Zhuang, et al., 2016, and references therein). However, whether the flux ropes are formed before or during their eruptions at the Sun is still a controversial issue on ICMEs (e.g., Jiang et al., 2016; Zhang et al., 2012). Song et al. (2016) used the time structure of iron average charge states ($Q_{\langle \text{Fe} \rangle}$) within MCs to resolve this problem, because the iron charge distribution is very sensitive to the heating processes near the Sun. They found that the time structure of $Q_{\langle \text{Fe} \rangle}$ can be classified into five types, that is, type A to type E. In type A, the time structure of $Q_{\langle \text{Fe} \rangle}$ displays a bimodal distribution with two peaks higher than 12, a threshold reasonable to indicate whether high iron charges states dominate. In type B, $Q_{\langle \text{Fe} \rangle}$ exhibits an unimodal distribution with one peak higher than 12; type C and type D show $Q_{\langle \text{Fe} \rangle}$ always higher and lower than 12, respectively. All other more complicated distributions are classified as type E. The different distributions imply different formation processes of twisted structures within MCs. As introduced above, the formation mechanism of SFRs is still unclear. We suppose that an investigation on the $Q_{\langle \text{Fe} \rangle}$ distributions in SFRs may further our understanding.

Generally, the heavy ion compositions, such as the charge states and elemental abundance ratios, are determined in the low corona, and they will not change as the solar wind propagates far out into the heliosphere (Fu et al., 2015; Lepri et al., 2013; von Steiger et al., 2000; Zhao et al., 2009). Therefore, the compositional measurements can reflect conditions of the solar wind source regions in the Sun (e.g., Zurbuchen, 2007, and references therein). However, so far, only a few investigations concentrated on the compositional characteristics of SFRs. Feng and Wang (2015) studied the alpha particle to proton density ratio (N_α/N_p), the oxygen charge states ratio (O^{7+}/O^{6+}), and $Q_{\langle \text{Fe} \rangle}$ in SFRs with ACE data. They found that some SFRs show enhanced N_α/N_p (≥ 0.06), high O^{7+}/O^{6+} (≥ 1), and high $Q_{\langle \text{Fe} \rangle}$ (≥ 12), implying their similar origin as MCs. By utilizing STEREO A data, Yu et al. (2016) investigated the $Q_{\langle \text{Fe} \rangle}$ variations in small transients, an extended range of SFRs, and they demonstrated that $Q_{\langle \text{Fe} \rangle}$ only increases in less than 5% of small transients. Moreover, Huang et al. (2017) traced a SFR, which is entrained by rolling back magnetic field lines, back to its source region in the cusp of the streamer belt with the support of N_α/N_p and heavy ion compositions. SFRs are more influenced than MCs by ambient solar wind due to their small sizes (Feng & Wang, 2015; Janvier et al., 2014a), but the $Q_{\langle \text{Fe} \rangle}$ variations, which are frozen-in within several solar radii, can be used to exclude propagation effects and provide evolutionary properties on the conditions at the origin (Huang et al., 2017; Lepri et al., 2013; von Steiger et al., 2000).

In this paper, we apply the method of Song et al. (2016) to study the $Q_{\langle \text{Fe} \rangle}$ distributions in SFRs and try to infer the formation processes of their twisted structures. In section 2, we introduce the data we used in this study. The observation and discussion are presented in section 3, and the main results are summarized in section 4.

2. Data

In this study, we use ACE data to investigate the $Q_{\langle \text{Fe} \rangle}$ distributions in SFRs. Three instruments onboard the ACE spacecraft provide the in situ data. The Solar Wind Electron, Proton, and Alpha Monitor (McComas et al., 1998) measures the solar wind plasma and suprathermal electrons. The Magnetic Field Experiment (C. Smith et al., 1998), and the Solar Wind Ion Composition Spectrometer (Gloeckler et al., 1998) provide the magnetic

Table 1
The Types of $Q_{<Fe>}$ Distributions in Small Flux Ropes During 1998 to 2009

Case No.	Date (YYYYMMDD)	SFR period (UT)	$Q_{<Fe>}$	Type
1	19980218	21:02–0219/07:40	T	C
2	19980306	15:02–22:04	F	D
3	19980516	02:48–07:28	T	B
4	19980615	15:43–22:47	NA	NA
5	19990830	06:38–10:48	F	D
6	19990922	21:40–0923/02:38	T	C
7	20000427	18:11–0428/00:13	NA	NA
8	20000726	02:54–07:24	T	E
9	20000919	09:05–13:42	T	C
10	20001011	01:51–08:54	F	D
11	20010109	09:57–15:02	F	D
12	20020712	00:46–08:19	F	D
13	20030117	07:26–12:41	F	D
14	20030510	05:56–10:45	T	B
15	20050220	00:01–05:14	F	D
16	20050531	19:19–0601/02:58	T	E
17	20060109	13:02–17:13	F	D
18	20060502	08:00–12:53	NA	NA
19	20060710	20:13–0711/02:35	F	D
20	20060916	01:57–07:13	F	D
21	20080322	14:48–19:43	F	D
22	20081017	20:05–1018/00:15	T	B
23	20090727	04:40–08:42	F	D
24	20091012	11:40–16:44	F	D
25	20091120	18:44–23:13	F	D

Note. T (F) means that a high $Q_{<Fe>}$ (≥ 12) value is (not) observed in a small flux rope (SFR), and NA suggests there is a gap of iron data.

field and solar wind compositional measurements, respectively. The plasma data have a time resolution of 64 s, the magnetic field data are derived from 16-s data, and the compositional parameters are hourly averages.

The SFRs from 1998 to 2009 are selected in our study. Feng and Wang (2015) listed the SFRs during 1998 to 2005 in their Table 1 using ACE data. These cases are identified primarily with two criteria: the magnetic field configurations can be approximately described with constant-alpha force-free flux ropes, that is, with the Lundquist solution (Lundquist, 1950), and the durations are no more than 12 hr and the diameters are less than 0.2 AU. Due to the 1-hr time resolution of heavy ion compositional data, the duration of SFRs is also required to be longer than 4 hr. Such SFRs are also called intermediate-size flux ropes (Feng et al., 2007). We use the same criteria to identify SFRs from 2006 to 2009. In our fitting program, we require the flux rope fitting quality χ_n , which is the normalized root-mean-square of the difference between the modeled results and observations (see equation (25) in Wang, Zhuang, et al., 2016), to be smaller than 0.5 for a justification of this choice see (Wang et al., 2015; Wang, Zhuang, et al., 2016). The boundaries are predominantly estimated with sharp changes on magnetic field configurations and plasma signatures (such as proton density, velocity, and temperature; Janvier et al., 2014a), and we also take into account the Lundquist fitting result to select the boundaries if the magnetic field and plasma characteristics are not clear. We also apply this method to recheck the cases from 1998 to 2005 listed in Feng and Wang (2015). However, we exclude eight cases, because one case (no. 17) lasts longer than 12 hr and seven more SFRs (Nos. 05, 08, 14–16, 18, and 20) are actually identified as part of long duration ICMs listed in Jian et al. (2006). After all, we decided to select the other cases with the same boundaries.

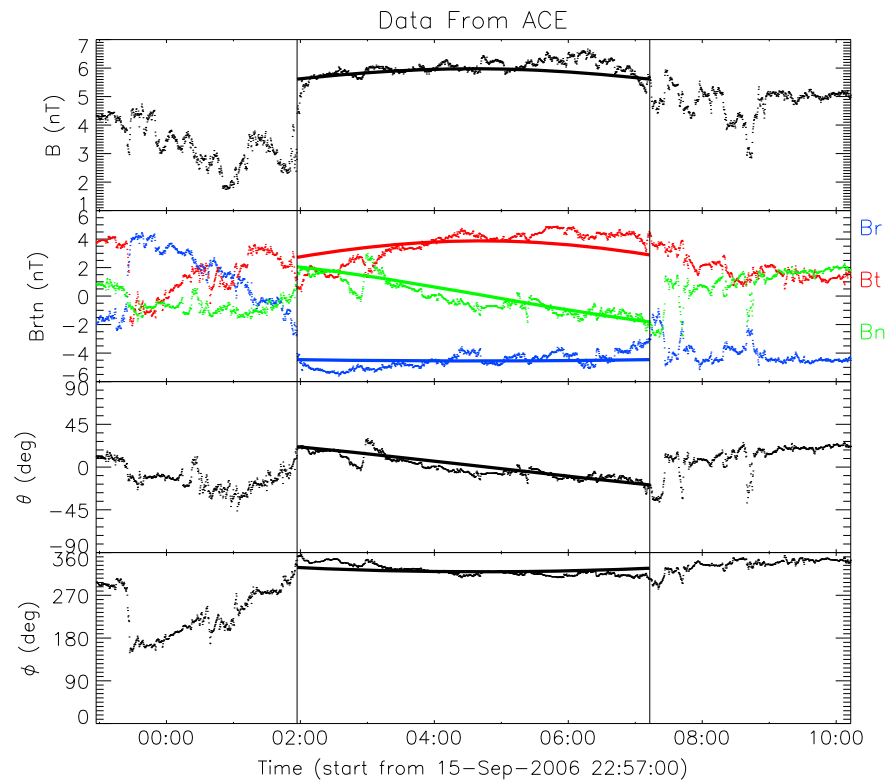


Figure 1. The Lundquist flux rope fitting results of a SFR observed by ACE. From top to bottom, the panels represent total magnetic field strength, magnetic field components, elevation angle, and azimuthal angle. The vertical lines indicate the boundaries of this SFR. The dots in each panel represent the observed values, and the overplotted solid lines represent the fitting values. SFR = small flux rope.

Figure 1 shows an example of the Lundquist flux rope fitting results of a SFR observed by ACE. From top to bottom, the panels represent total magnetic field strength, magnetic field components, elevation angle θ , and azimuthal angle ϕ . As indicated by the vertical lines, this SFR was observed from 01:57 to 07:13 UT on 16 September 2006. During this time period, the Lundquist fitting results (solid lines) overlay the observed values (dots). Obviously, both θ and ϕ rotate smoothly and the magnetic field components are fitted well by the modeled fields ($\chi_n = 0.21$). The fit parameters suggest this SFR is a left-handed flux rope, and its axial direction is 57.47° in longitude and 2.10° in latitude in RTN coordinates. Besides, the estimated field strength at the axis is 10.83 nT.

3. Observation and Discussion

3.1. $Q_{\langle \text{Fe} \rangle}$ Distributions

Figure 2 shows examples of different types of $Q_{\langle \text{Fe} \rangle}$ distributions. Figure 2a presents a type B example (one $Q_{\langle \text{Fe} \rangle}$ peak higher than 12) observed on 16 May 1998, with the vertical dashed lines marking its boundaries. The first and second panels denote the magnetic field components and azimuthal angle, respectively. The third panel indicates the fractional distribution of iron charge states with 2-hr time resolution, and the fourth panel represents the variations of $Q_{\langle \text{Fe} \rangle}$ with one σ statistical error bars added. Even though the fractional distributions have a lower time resolution, they clearly show the variation of the predominant charge states. In this figure, the last two panels clearly denote that the enhanced $Q_{\langle \text{Fe} \rangle}$ (≥ 12) displays one peak in this SFR, when the dominant charge state is 16; that is, it is a type B distribution. Similarly, Figures 2b and 2c showcase SFRs with $Q_{\langle \text{Fe} \rangle}$ always larger and smaller than 12, that is, type C and type D, respectively.

Figure 3 shows two cases of type E distributions. As shown in Figure 3a, $Q_{\langle \text{Fe} \rangle}$ is only slightly enhanced at the front boundary for a short time and then decreases to values lower than 12. Furthermore, the fractional distributions clearly suggest that high iron charge states contribute much less to $Q_{\langle \text{Fe} \rangle}$ at the rear boundary than at the front boundary. The more variable case in Figure 3b, which has been displayed in Feng and Wang (2015), denotes triple peaks with $Q_{\langle \text{Fe} \rangle}$ slightly larger than 12. We note that the three peaks in this case are

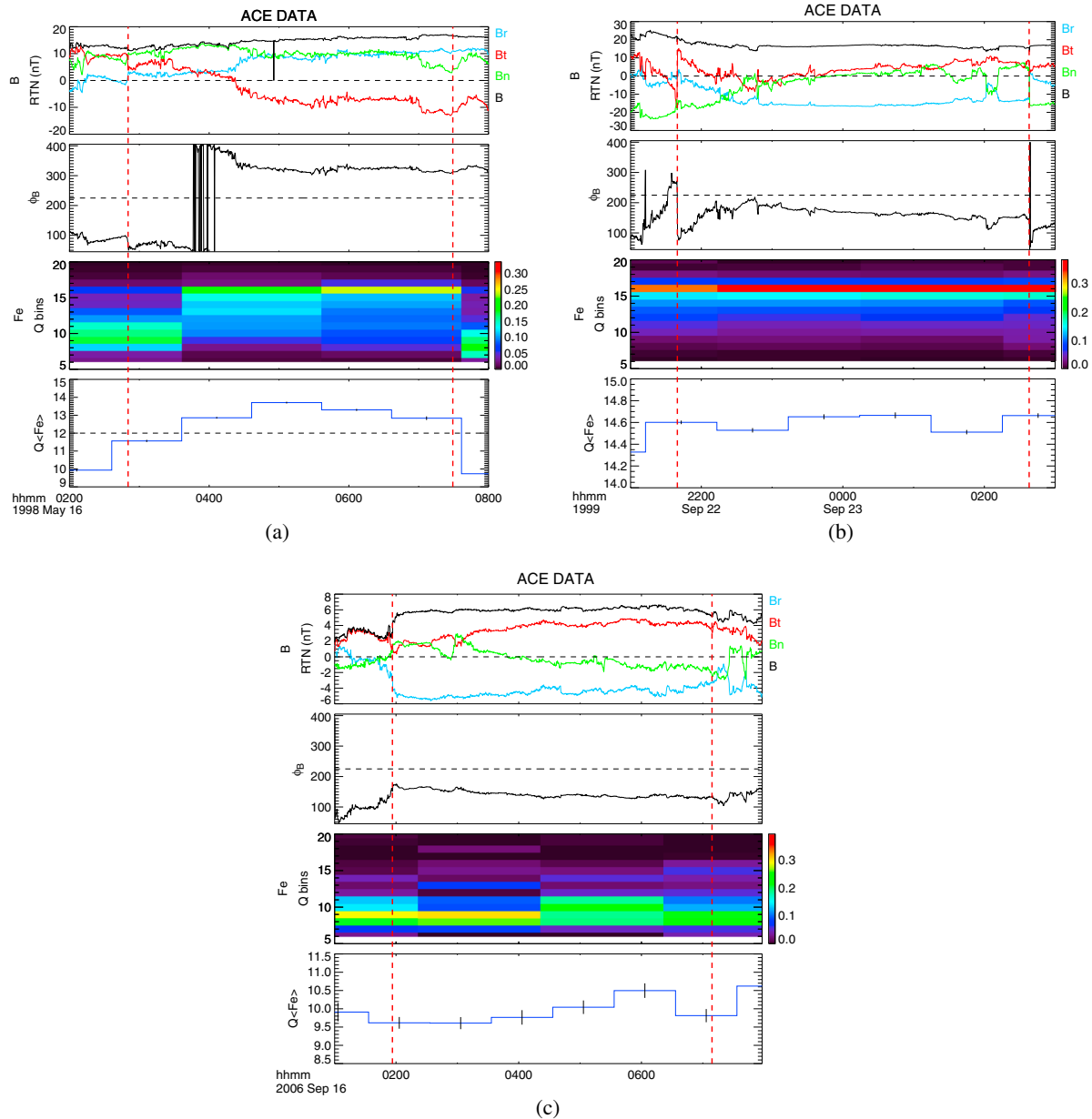


Figure 2. Examples of different types of $Q_{\langle Fe \rangle}$ distributions. (a) Example of a type B distribution; (b) example of a type C distribution; (c) example of a type D distribution. From top to bottom, the panels represent magnetic field components in RTN coordinates, azimuthal angle, the fractional distribution of iron charge states (2-hr time resolution), and the average charge states of iron $Q_{\langle Fe \rangle}$ (1-hr time resolution). The one σ error bars of $Q_{\langle Fe \rangle}$ are also added in the last panel of each figure. The dashed vertical lines in each figure mark the boundaries of small flux ropes.

not that pronounced, but there are definitely contributions of high iron charge states as shown by the fractional distributions. Therefore, we classify it as type E based on these data. These cases may imply complicated formation processes.

Table 1 lists the 25 SFRs and their corresponding types of $Q_{\langle Fe \rangle}$ distributions from 1998 to 2009. The first column shows the case number. The second and third columns indicate the observed time of SFRs. In the fourth column, T demonstrates that a high $Q_{\langle Fe \rangle}$ (≥ 12) value is observed in a SFR, F means no such signature. Due to the generally short durations of SFRs and the 1-hr time resolution $Q_{\langle Fe \rangle}$ data, in practice, T means there was at least one point higher than 12. The last column presents the types of $Q_{\langle Fe \rangle}$ distributions following the classification of Song et al. (2016). Furthermore, the data in the first to fourth columns of the top 16 SFRs come from Feng and Wang (2015).

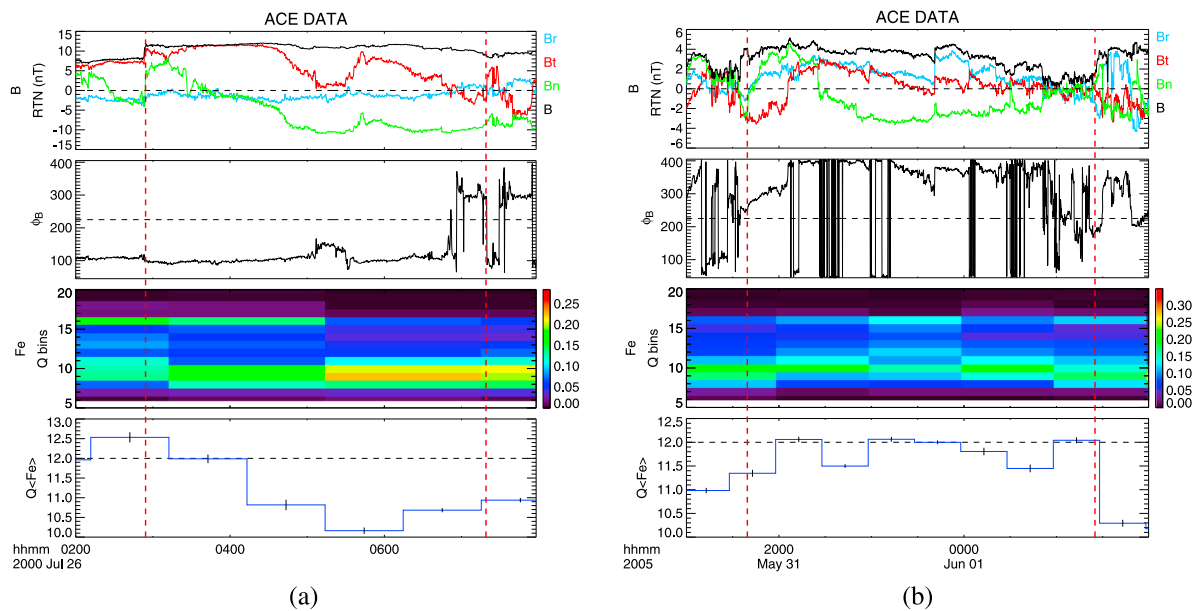


Figure 3. Two cases of type E distributions, in the same format as Figure 2.

Among the 25 cases, three cases have a gap on iron data (*NA*). Eight out of the other cases display an enhanced $Q_{<Fe>}$, and their types are type B (three cases, 13.6%), type C (three cases, 13.6%), and type E (two cases, 9.2%). The other 14 cases (63.6%) do not show any enhanced $Q_{<Fe>}$; that is, they are type D. No type A distributions are observed, which is different from MCs. This is the most conspicuous signature and will be discussed later. In addition, the enhanced $Q_{<Fe>}$ appears more frequent in the SFRs observed from 1998 to 2005. This may be associated with solar activity, which is consistent with the result for MCs (Song et al., 2016).

There could be some uncertainties to determine the boundaries of SFRs, but such uncertainties should have limited influence on the categorization in this study. There are 17 out of 22 cases with $Q_{<Fe>}$ either larger or smaller than 12 (type C and type D), and these cases have such signatures extending beyond their boundaries; that is, a small shift of boundaries will not change their types. In addition, two type E cases (as shown in Figure 3) and three type B cases generally show good boundaries that are well identified by the sharp changes of magnetic field components and plasma signatures. Thus, even if some SFR boundaries are slightly changed, the categorization will not be significantly affected.

3.2. Possible Origin

SFRs have two types of possible source regions, and different origins may affect the formation of different types. Therefore, it is necessary to investigate the possible origin of these SFRs. As introduced above, SFRs are sensitive to the influences of ambient environment in the heliosphere, thus their source regions are difficult to identify. The imaging observations may provide direct evidences, but this method is generally based on appropriate conditions (such as SFRs should be entrained by corotating interaction regions; e.g., Rouillard et al., 2009, 2011), which may reduce the accuracy. Several studies investigated the source regions of SFRs using in situ characteristics (e.g., Cartwright & Moldwin, 2008; Feng & Wang, 2015; Feng et al., 2015; Janvier et al., 2014b; Tian et al., 2010; Yu et al., 2016, 2014); however, they generally relied on statistical results. Consequently, it is difficult to identify the source region of a specific SFR without sufficiently utilizing the compositional signatures of individual SFRs. In this study, we add N_{α}/N_p and $Q_{<Fe>}$ to help to locate the possible origins of these 25 SFRs.

Magnetic reconnection exhaust at the boundary of a SFR implies its interactions with ambient solar wind (Tian et al., 2010). N_{α}/N_p and charge states of heavy ions are generally enhanced in MCs, although both are not necessarily simultaneously enhanced (Feng & Wang, 2015; Richardson & Cane, 2004, and references therein). Thus, if a SFR is originating from the magnetic erosion of a MC, magnetic reconnection exhaust at one or both boundaries is indispensable. In addition, we use the more strict requirement of both high $Q_{<Fe>}$ (≥ 12) and enhanced N_{α}/N_p (≥ 0.06) to relate such SFRs to MCs. In this study, the primary criteria to identify a magnetic reconnection exhaust are used as given by Tian et al. (2010): (1) an obvious plasma jet within a region with

magnetic field rotations and (2) at least one component of both the velocity change and the magnetic field change is correlated on one side and anticorrelated on the other side. In addition, nearly 90% of the SFRs that appear far away from HCSs have counterstreaming suprathermal electrons (CSEs), but those adjacent to HCSs do not always show CSEs (Feng et al., 2015). The CSEs reveal that the suprathermal electrons stream along the magnetic field, both in parallel and antiparallel directions, implying closed magnetic field lines (e.g., Huang, Liu, Qi, et al., 2016; Lavraud et al., 2010). Therefore, we suggest that the SFRs originating from HCSs should satisfy the following criteria: a HCS in the vicinity, no CSEs, and N_α/N_p is smaller than 0.06 but larger than 0.02. Then, the other SFRs are believed to originate from the solar corona. The plasma blobs that formed from the closed region of the streamer belt are suggested to show depleted alpha particle abundance ($N_\alpha/N_p \leq 0.02$) in the vicinity of HCSs (Suess et al., 2009), but in situ data still cannot separate the plasma blobs from jets efficiently. Because the charge states are frozen-in below a few solar radii, we are unable to distinguish their source regions with compositional characteristics. In general, the above criteria are somewhat strict to identify SFRs that originate from HCSs and erosion of MCs. For example, the magnetic reconnection exhausts may not be observed because the erosion of MCs could have happened inside 1 AU, but the spacecraft may not encounter them near 1 AU. Similarly, magnetic reconnection is involved in the HCS, but we do not require magnetic reconnection exhaust to be a signature for HCS associated events. That is because we can identify HCS associated events without exhausts, but we cannot identify erosion associated events without them. Besides, HCS associated events may not always relate to the absence of CSEs as suggested by Feng et al. (2015). However, due to the multiple origins of SFRs, we decide to use more strict criteria to identify the most probable sources of these SFRs.

Figure 4 shows an example of SFR (no. 6) with CSEs and magnetic reconnection exhaust. The $Q_{<Fe>}$ characteristics have been presented in Figure 2b. In this SFR, the fifth panel suggests that the azimuthal angle is around 160° ; that is, the magnetic field lines are directed sunward. Thus, the suprathermal electrons should predominantly concentrate on pitch angle 180° as they always flow antisunward. However, the first panel obviously reveals that a large number of suprathermal electrons also flow along pitch angle 0° at the same time, implying counterstreaming signatures. Besides, the shaded region following the rear boundary of this SFR shows a magnetic reconnection exhaust from 02:33 to 02:41 UT on 23 September 1999. A clear decrease of magnetic field strength is observed in the reconnection exhaust. The plasma jet and magnetic field rotation mainly appear in t and n directions in the RTN coordinates. In these directions, the changes of magnetic field vectors and plasma velocity vectors denote a clear anticorrelation at the leading side and a correlation at the rear side of the reconnection exhaust. Other signatures of magnetic reconnection (such as the local increase of plasma beta, proton density and temperature) are also observed.

Using the above criteria, Table 2 presents the possible origins of the 25 SFRs. The first and second columns show the case number and observation date, the same as in Table 1. In the third column, F indicates that there is no magnetic reconnection exhaust, and L (R) next to the time period denotes the reconnection exhaust appears at the leading (rear) boundary. The average value of N_α/N_p in each SFR is presented in the fourth column. Due to ACE data gaps in some SFRs, N_α/N_p values are derived for the available part of the SFR time period or from data of the Wind spacecraft if it observed the same case. The fifth column shows the crossing time of HCSs in the vicinity of SFRs, with F marking no HCS crossing. The sixth column shows the percentage of CSEs in each SFR, evaluated with an automated procedure as follows. The Solar Wind Electron, Proton, and Alpha Monitor instrument provides the suprathermal electron pitch angle distribution functions at the energy of 272 eV as shown in Figure 4. We first calculate the distribution functions near pitch angle 0° , 90° and 180° , and each of them includes five pitch angle bins with a width of about 8° each. If the distribution functions near pitch angle 0° and 180° are both larger than the value at pitch angle 90° , then the CSE is identified (e.g., Lavraud et al., 2010). We require the CSE to cover more (less) than 10% of the event, marked by T (F), to be a (no) signature of typical CSEs in the SFRs. The appearance of CSEs seems to be more frequent with our automated selection method (92%) than with the manual method (75%) of Feng et al. (2015). In the last column, *erosion*, *HCS* and *corona* signify that the SFRs are originating from magnetic erosion of MCs, HCSs, and solar corona, respectively.

Tian et al. (2010) suggested that 42% of SFRs have magnetic reconnection exhausts at the boundaries, and their appearance probabilities are comparable at both sides. From the third column in this table, we can find that eight cases (32%) have a reconnection exhaust at the boundary, and half of them appear at the leading or rear boundary, consistent with Tian et al. (2010). Besides, we find that 12 SFRs (48%) occur in the vicinity of HCSs, which is also consistent with the previous results (46%) of Feng et al. (2015).

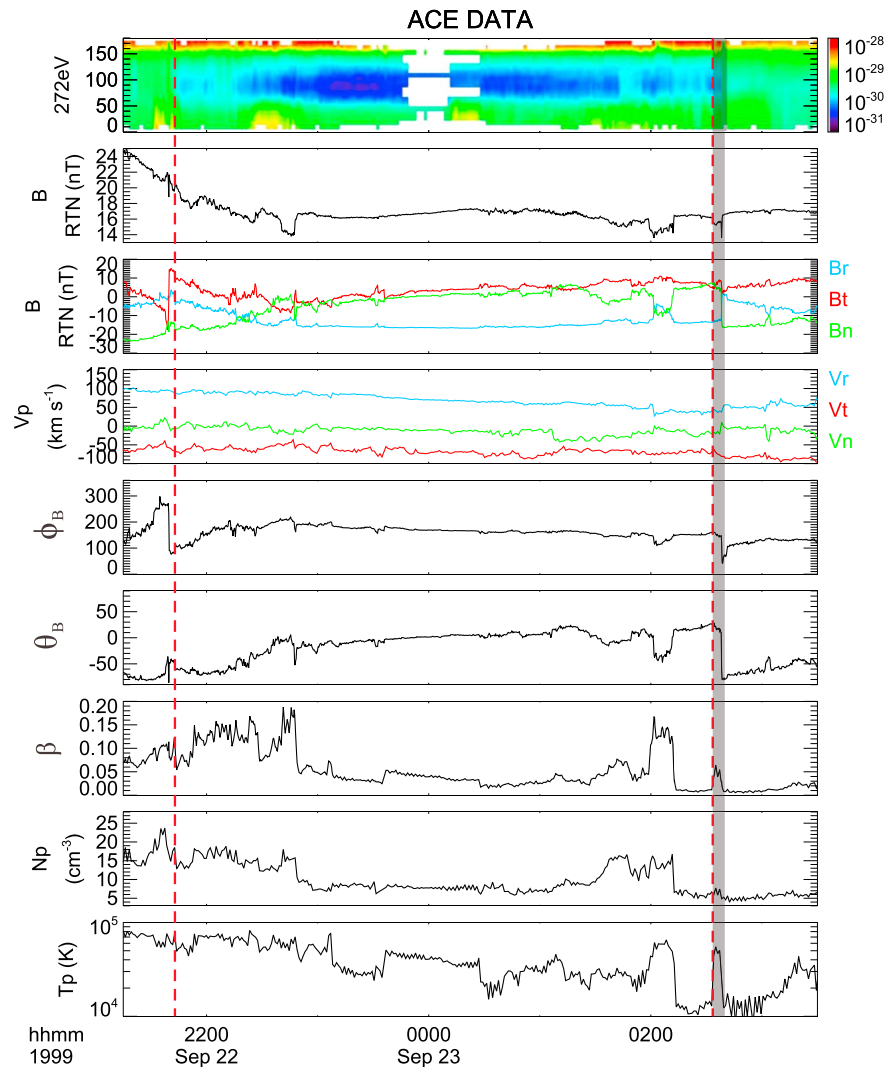


Figure 4. An example of SFR with counterstreaming suprathermal electrons and magnetic reconnection exhaust. From top to bottom, the panels show pitch angle distributions of suprathermal electrons at 272 eV, magnetic field strength, magnetic field components, plasma velocity vectors, magnetic field azimuthal angle, elevation angle, plasma beta, proton density, and temperature. A value of 500 km/s has been subtracted from the r component velocity. Two dashed vertical lines mark the beginning and end of this SFR. The shaded region denotes the crossing of magnetic reconnection exhaust. SFR = small flux rope.

Combining Tables 1 and 2, we present the results of the classification by $Q_{<Fe>}$ types and the possible origins of these SFRs in Table 3. We find that three SFRs are formed by the magnetic erosion of MCs. Two of them show type C distributions, and one case displays type E distributions. Seven SFRs originate from the vicinity of HCSs. One and five cases exhibit type B and type D distributions, respectively, and one case cannot be classified because of a gap in $Q_{<Fe>}$ data. The other 15 cases are released from the solar corona. Type D dominates with nine cases. Type B has two cases, type C and type E have only one case each, and the other two cases have a data gap. From this table, it seems SFRs originating from the interplanetary medium are somewhat less than those from the solar corona.

3.3. Discussion

In this section, the formation mechanisms of $Q_{<Fe>}$ distributions will be discussed based on the comparisons between the above results and previous results on MCs.

For MCs, Song et al. (2016; as shown in Figure 5) suggested that a low ionized core ($Q_{<Fe>} \leq 12$) would exist within the MCs if their twisted structures are formed prior to the eruptions, and the then formed current sheets

Table 2*The Possible Origins of the Small Flux Ropes During 1998 to 2009*

Case No.	Date (YYYYMMDD)	Reconnection exhaust	N_{α}/N_p	HCS	CSE (> 10%)	Possible origin
1	19980218	F	0.051 ^a	F	F (8.3%)	corona
2	19980306	F	0.065	03/04 14:35	F (0.0%)	HCS
3	19980516	F	0.033	05/15 15:58	F (6.5%)	HCS
4	19980615	F	0.009 ^a	F	T (45.1%)	corona
5	19990830	F	0.043	08/30 03:15	T (41.9%)	corona
6	19990922	(R) 02:33-02:41	0.076	09/22 12:28	T (100%)	erosion
7	20000427	F	0.055	04/27 07:41	F (7.0%)	HCS
8	20000726	F	0.041	F	F (7.7%)	corona
9	20000919	(R) 13:42-13:50	0.094	F	T (91.3%)	erosion
10	20001011	(R) 08:54-10:37	0.047 ^b	10/08 12:35	F (9.2%)	HCS
11	20010109	F	0.046	01/10 19:42	F (2.3%)	HCS
12	20020712	F	0.050	07/12 03:21	F (9.4%)	HCS
13	20030117	F	0.047	01/17 12:41	F (0.4%)	HCS
14	20030510	(L) 05:48-05:56	0.018	F	T (66.3%)	corona
15	20050220	F	0.027	F	T (85.3%)	corona
16	20050531	(L) 19:05-19:19	0.072	F	T (66.6%)	erosion
17	20060109	(R) 17:13-17:17	0.016 ^b	F	F (0.0%)	corona
18	20060502	F	0.004 ^b	F	T (11.9%)	corona
19	20060710	F	0.025 ^b	07/11 14:38	T (89.4%)	corona
20	20060916	(L) 01:26-01:57	0.011 ^b	09/16 12:14	T (68.4%)	corona
21	20080322	F	0.022	F	F (0.7%)	corona
22	20081017	F	0.001 ^b	10/17 19:44	T (21.3%)	corona
23	20090727	(L) 04:29-04:40	0.002	F	F (7.2%)	corona
24	20091012	F	0.003 ^a	F	T (27.0%)	corona
25	20091120	F	0.023	F	F (6.1%)	corona

Note. *T* and *F* mean the presence and absence of a signature (reconnection exhaust, HCS and CSE), respectively. *L* and *R* indicate that reconnection exhaust appears at the leading and rear boundary of a SFR, respectively. HCS = heliospheric current sheet; CSE = counterstreaming suprathermal electron; SFR = small flux rope.

^a The values are derived from the part of the SFR time period covered by ACE data. ^b Due to ACE data gap, the N_{α}/N_p values are derived from data of Wind spacecraft, which observed the same SFRs.

during the eruptions could be of high or normal temperatures, which correspond to high or low iron ionization states, respectively. As a consequence, the two conditions and the crossing trajectory of spacecraft may result in different types of $Q_{<Fe>}$ distributions in the observations. Following Song et al. (2016), it is obvious from Figure 5 that MCs with type A distributions have their twisted structures formed prior to eruptions. Type B distributions are related to temperature variations of current sheets during eruptions, but type C are related

Table 3*The $Q_{<Fe>}$ Types and the Possible Origins of Small Flux Ropes*

	Magnetic erosion	HCS	Solar corona
Type B	0	1	2
Type C	2	0	1
Type D	0	5	9
Type E	1	0	1
DATA GAP	0	1	2
Total	3	7	15

Note. HCS = heliospheric current sheet.

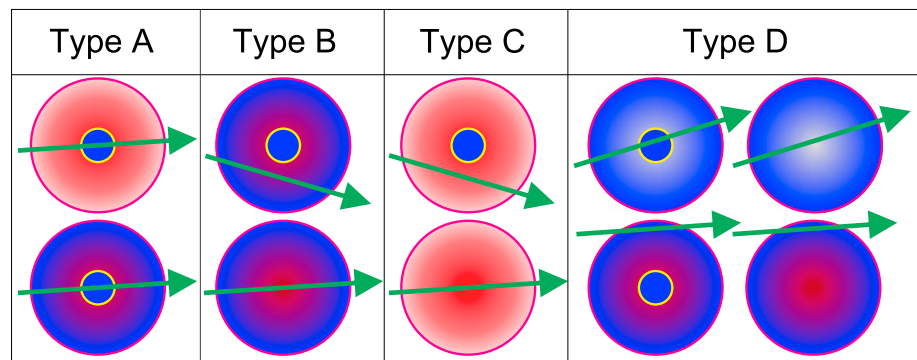


Figure 5. Schematic figure to explain the $Q_{\langle \text{Fe} \rangle}$ distributions in MCs, derived from Song et al. (2016). Blue and red colors represent low and high iron ionization states, respectively. The inner blue circles indicate a low ionized core in MCs. The green lines with arrow show the crossing trajectory of spacecraft. MC = magnetic cloud.

to high-temperature current sheets. However, an appropriate crossing trajectory through the MCs with a low ionized core could also display type B or type C in the observations. Type D distributions generally relate to low-temperature current sheets, which may be associated with reconnection processes in the lower atmosphere, or crossing through the boundaries of SFRs that have variable $Q_{\langle \text{Fe} \rangle}$ distributions inside the MCs. Type E suggests nonuniform distributions of $Q_{\langle \text{Fe} \rangle}$ within MCs. Similar to the case no. 8 as shown in Figure 3a, Song et al. (2016) also found the $Q_{\langle \text{Fe} \rangle}$ in one case decreasing from high to low level, and this could be a manifestation of cold filament material in MCs (Song et al., 2017). However, cases with three peaks higher than 12 (similar to case no. 16 in Figure 3b) are still unclear.

SFRs originating from the solar corona show types B–E distributions. Because these SFRs have similar origins as MCs, they are expected to include all types of $Q_{\langle \text{Fe} \rangle}$ distributions. The fact that no type A distributions are observed seems to be the most distinct difference between SFRs and MCs. Types B–D distributions can also be associated with twisted structures that formed before eruptions, if the spacecraft trajectory does not cross the low ionized core, or the current sheets should have normal temperatures (see the first condition for type D in Figure 5). However, based on the ratio of the closest approach distance to the radius (d_0/R_0) of 144 SFRs from Feng et al. (2007), we find from their Table 1 that more than 20% of SFRs cross the spacecraft through positions very close to the center ($d_0/R_0 \leq 0.1$). Even though the sizes of the low ionized cores are still unknown, the fact that no type A is observed may imply the twisted structures of these SFRs are generally formed during their eruptions.

SFRs in the vicinity of HCSs only show type B and type D distributions. Solar wind in the vicinity of HCSs is generally slow speed (e.g., Y. Liu et al., 2014; Peng et al., 2017), which generally shows low $Q_{\langle \text{Fe} \rangle}$ (Abbo et al., 2016; Lepri et al., 2001). As the charge states of heavy ions are frozen-in below a few solar radii, $Q_{\langle \text{Fe} \rangle}$ is not expected to be changing in the interplanetary medium. Therefore, type D dominating the $Q_{\langle \text{Fe} \rangle}$ distributions of this type of SFRs is reasonable. In addition, slow solar wind occasionally shows enhanced $Q_{\langle \text{Fe} \rangle}$ (e.g., Abbo et al., 2016; Zhao et al., 2017), then type B is possible as multiple magnetic reconnection proceeds with such solar wind in the vicinity of HCSs.

SFRs that formed through magnetic erosion of MCs include type C and type E distributions. Obviously, the $Q_{\langle \text{Fe} \rangle}$ types of these SFRs are connected to those of MCs. Magnetic erosion peels off the outside portion of MCs; therefore, it is easy to understand that these SFRs have type C distributions. However, type A and type B distributions are present in MCs, but they are not observed in SFRs. This result implies that the erosion may peel off all the portions of MCs that surround the low ionized core, which leads to an exclusion of these cases from magnetic erosion category as we require such cases should have high $Q_{\langle \text{Fe} \rangle}$. This is possible according to current numerical studies, suggesting magnetic erosion could reduce about 37% of the original MC flux, and nearly 60% are reduced when a fast shock hits the MC (Mao et al., 2017). If the spacecraft trajectory crosses the SFR near the boundary and/or the related MCs have their twisted structures formed during eruptions, then type A distributions should not be observed either. Furthermore, type B distributions could also disappear if there is no temperature variation of the current sheets associate with the MCs eruptions. Besides, the fact that type D is not observed could be due to our strict selection criteria that both $Q_{\langle \text{Fe} \rangle}$ and N_α/N_p should be enhanced, which may not be the circumstance simultaneously in MCs (Richardson & Cane, 2004).

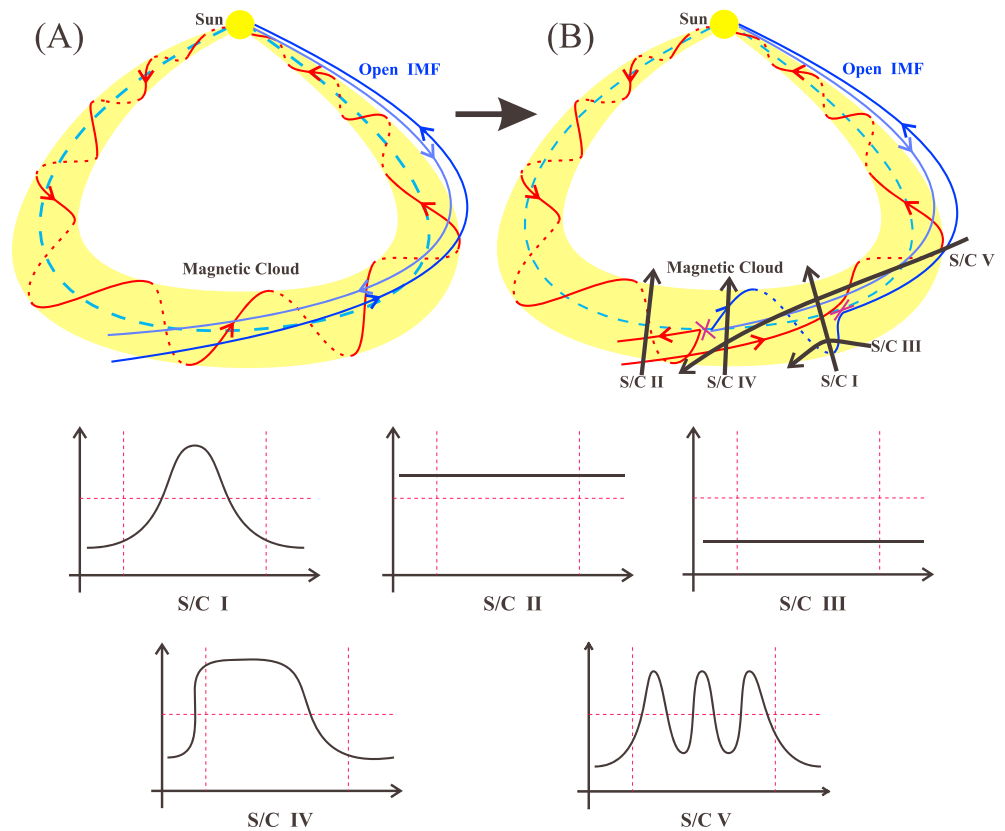


Figure 6. Schematic figures to illustrate the magnetic erosion of MCs, derived from Ruffenach et al. (2012). The yellow cylinders with red helical lines represent MCs. Blue lines indicate open magnetic field lines that participate in magnetic reconnection with MCs. Red and blue colors indicate high and low $Q_{<Fe>}$, respectively. Panel (a) shows the original configurations of MCs, and the corresponding results after magnetic erosions by reconnection are displayed in panel (b). The bold black lines denote the schematic crossing trajectories of spacecraft with the direction indicated by the arrow, and the expected $Q_{<Fe>}$ variations in observations are presented in the lower charts, with the horizontal dashed lines indicating $Q_{<Fe>} = 12$ and vertical dashed lines marking the boundaries of small flux ropes. MC = magnetic cloud; IMF = interplanetary magnetic field.

Besides, case no. 16 implies that magnetic erosion may play a role in the formation of type E cases with three peaks higher than 12. Such $Q_{<Fe>}$ distributions in MCs are difficult to understand when only considering $Q_{<Fe>}$ variations near the Sun. This case suggests that magnetic erosion in interplanetary space may contribute. MCs generally have enhanced $Q_{<Fe>}$, but along the open magnetic field lines may stream out solar wind with high or low $Q_{<Fe>}$. If magnetic erosion happens between MC and magnetic field lines with high $Q_{<Fe>}$, then the resulting $Q_{<Fe>}$ distributions should not be changed significantly. However, if the open magnetic field lines carry low $Q_{<Fe>}$, which is common, the situation could be different. Figure 6 shows such a scenario that is derived from Ruffenach et al. (2012). Figures 6a and 6b show a schematic configuration before and after erosion, where a MC is eroded by magnetic field lines with different polarities. The $Q_{<Fe>}$ variations are assumed to be consistent with the source regions of magnetic field lines as marked by red (high charge states) and blue (normal charge states) colors. The observer may cross the flux rope through different trajectories, that is, S/C I–V, and the corresponding $Q_{<Fe>}$ variations are presented in the lower charts. S/C I–III represent types B–D distributions, respectively. S/C IV reproduces a type E distribution with $Q_{<Fe>}$ decreasing from high to low values, which is similar to that of case no. 8. If the observer crosses the flux rope with the trajectory of S/C V, another type E distribution with three peaks higher than 12 could be formed. The S/C V crossing trajectory may not be realistic, but such a conceptual scenario provides clues for the possible formation mechanism for such cases like no. 16, because the magnetic erosion could be more complex than we present here. Besides, apparently type A distributions, with only two peaks higher than 12, may also be possible with an appropriate crossing trajectory.

The above analyses indicates that the formation mechanism of different $Q_{<Fe>}$ distributions may relate to their origins. However, because the time resolution of $Q_{<Fe>}$ data is only 1 hr, we only choose cases with durations longer than four hours. It means that our study of $Q_{<Fe>}$ distributions in SFRs is currently limited to a subset of SFRs, that is, *intermediate*-sized flux ropes. Therefore, we cannot preclude the possibility that events shorter than four hours, which represent about 75% of total SFRs as suggested by Cartwright and Moldwin (2008), could have different behaviors. If we assume that SFRs have similar $Q_{<Fe>}$ distributions as MCs and Song et al. (2016) find that type A dominates about 12% of MCs, then only about two SFRs could be observed as estimated with our samples. However, the spacecraft may just miss such SFRs due to their small sizes and/or they are easily influenced by ambient environment. Besides, type A distributions may just happen to be concealed by the low-resolution data. With high time resolution data obtained from future missions (such as Parker Solar Probe and Solar Orbiter missions), a more precise investigation could be possible.

4. Conclusion

In this study, $Q_{<Fe>}$ distributions in SFRs are investigated to understand the formation mechanism of twisted structures of SFRs. With ACE data, 25 cases and their $Q_{<Fe>}$ types are identified. Compared to previous studies, we use additional compositional parameters (N_{α}/N_p and $Q_{<Fe>}$) to trace the possible source regions of these SFRs with in situ data. Combining the $Q_{<Fe>}$ distributions with possible sources of the SFRs, we further analyze the formation mechanisms of both the twisted structures and $Q_{<Fe>}$ types of SFRs.

Based on the observations, types B–E distributions of $Q_{<Fe>}$ are found in SFRs, but type A distributions are not observed. With our modified criteria, the SFRs are reconfirmed to have two source regions, that is, solar corona and interplanetary space. However, in comparison with MCs, our analysis suggests that the twisted structures of the SFRs originating from the solar corona may be formed predominately during their eruptions. For the SFRs originating from interplanetary space, the $Q_{<Fe>}$ distributions are much more complex, and magnetic erosions of MCs may play an important role in forming intricate type E distributions through the reconfiguration of the magnetic field topology.

Acknowledgments

This work is supported by the Chinese National Science Foundation of contract 41674173, the Chinese Academy of Sciences *Hundred Talented Program* of contract Y32135A47S, and the Specialized Research Fund for State Key Laboratory of China. We thank the ACE teams for the in situ data. The Lundquist fitting results are derived from DREAMS flux rope model (<http://space.ustc.edu.cn/dreams/>) (http://space.ustc.edu.cn/dreams/mc_fitting/), which is generated and maintained by the team of Solar-Terrestrial Exploration and Physics (STEP) at University of Science and Technology of China (USTC). We also acknowledge the online small-scale magnetic flux rope database (via www.fluxrope.info/), generated and maintained by Jinlei Zheng and Qiang Hu at University of Alabama in Huntsville. We appreciate the valuable suggestions from Hui Tian and Jiansen He.

References

- Abbo, L., Ofman, L., Antiochos, S., Hansteen, V., Harra, L., Ko, Y.-K., et al. (2016). Slow solar wind: Observations and modeling. *Space Science Reviews*, 201, 55–108.
- Burlaga, L., Sittler, E., Mariani, F., & Schwenn, R. (1981). Magnetic loop behind an interplanetary shock: Voyager, Helios, and IMP 8 observations. *Journal of Geophysical Research*, 86(A8), 6673–6684. <https://doi.org/10.1029/JA086iA08p06673>
- Cartwright, M., & Moldwin, M. (2008). Comparison of small-scale flux rope magnetic properties to large-scale magnetic clouds: Evidence for reconnection across the HCS? *Journal of Geophysical Research*, 113, A09105. <https://doi.org/10.1029/2008JA013389>
- Chen, Y., Li, X., Song, H., Shi, Q., Feng, S., & Xia, L. (1936). Intrinsic instability of coronal streamers. *Astronomy Journal*, 691.
- De Pontieu, B., van der Voort, L. R., McIntosh, S., Pereira, T., Carlsson, M., Hansteen, V., et al. (2014). On the prevalence of small-scale twist in the solar chromosphere and transition region. *Science*, 346, 1255732.
- Feng, H., & Wang, J. (2015). Observations of several unusual plasma compositional signatures within small interplanetary magnetic flux ropes. *Astronomy Journal*, 809, 112.
- Feng, H., & Wu, D. (2009). Observations of a small interplanetary magnetic flux rope associated with a magnetic reconnection exhaust. *Astronomy Journal*, 705, 1385–1387.
- Feng, H., Wu, D., & Chao, J. (2007). Size and energy distributions of interplanetary magnetic flux ropes. *Journal of Geophysical Research*, 112, A02102. <https://doi.org/10.1029/2006JA011962>
- Feng, H., Zhao, G., & Wang, J. (2015). Counterstreaming electrons in small interplanetary magnetic flux ropes. *Journal of Geophysical Research: Space Physics*, 120, 10,175–10,184. <https://doi.org/10.1002/2015JA021643>
- Forbes, T. (2000). A review on the genesis of coronal mass ejections. *Journal of Geophysical Research*, 105(A10), 23,153–23,165. <https://doi.org/10.1029/2000JA000005>
- Fu, H., Li, B., Li, X., Huang, Z., Mou, C., Jiao, F., & Xia, L. (2015). Coronal sources and in situ properties of the solar winds sampled by ace during 1999–2008. *Solar Physics*, 290, 1399–1415.
- Gloeckler, G., Cain, J., Ipavich, F., Tums, E., Bedini, P., Fisk, L., et al. (1998). Investigation of the composition of solar and interstellar matter using solar wind and pickup ion measurements with SWICS and swims on the ACE spacecraft. *Space Science Reviews*, 86(1–4), 497–539.
- Gold, T., & Hoyle, F. (1960). On the origin of solar flares. *Monthly Notices of the Royal Astronomical Society*, 120(2), 89–105.
- Gosling, J., Skoug, R., McComas, D., & Smith, C. (2005). Magnetic disconnection from the Sun: Observations of a reconnection exhaust in the solar wind at the heliospheric current sheet. *Geophysical Research Letters*, 32, L05105. <https://doi.org/10.1029/2005GL022406>
- He, J., Zhu, X., Chen, Y., Chadi, S., Michael, S., Li, H., et al. (2018). Plasma heating and Alfvénic turbulence enhancement during two steps of energy conversion in magnetic reconnection exhaust region of solar wind. *Astronomy Journal*, 856, 148.
- Hu, H., Liu, Y. D., Wang, R., Möstl, C., & Yang, Z. (2016). Sun-to-Earth characteristics of the 2012 July 12 coronal mass ejection and associated geo-effectiveness. *Astronomy Journal*, 829, 97.
- Hu, Q., & Sonnerup, B. U. (2001). Reconstruction of magnetic flux ropes in the solar wind. *Geophysical Research Letters*, 28(3), 467–470. <https://doi.org/10.1029/2000GL012232>
- Hu, Q., & Sonnerup, B. U. (2002). Reconstruction of magnetic clouds in the solar wind: Orientations and configurations. *Journal of Geophysical Research*, 107(A7), 1142. <https://doi.org/10.1029/2001JA000293>
- Huang, J., Liu, Y. C.-M., Klecker, B., & Chen, Y. (2016). Coincidence of heliospheric current sheet and stream interface: Implications for the origin and evolution of the solar wind. *Journal of Geophysical Research: Space Physics*, 121, 19–29. <https://doi.org/10.1002/2015JA021729>

- Huang, J., Liu, Y. C.-M., Peng, J., Li, H., Klecker, B., Farrugia, C. J., et al. (2017). A multispacecraft study of a small flux rope entrained by rolling back magnetic field lines. *Journal of Geophysical Research: Space Physics*, 122, 6927–6939. <https://doi.org/10.1002/2017JA023906>
- Huang, J., Liu, Y. C.-M., Qi, Z., Klecker, B., Marghitu, O., Galvin, A. B., et al. (2016). A multievent study of the coincidence of heliospheric current sheet and stream interface. *Journal of Geophysical Research: Space Physics*, 121, 10,768–10,782. <https://doi.org/10.1002/2016JA022842>
- Janvier, M., Démoulin, P., & Dasso, S. (2014a). In situ properties of small and large flux ropes in the solar wind. *Journal of Geophysical Research: Space Physics*, 119, 7088–7107. <https://doi.org/10.1002/2014JA020218>
- Janvier, M., Démoulin, P., & Dasso, S. (2014b). Are there different populations of flux ropes in the solar wind? *Solar Physics*, 289, 2633–2652.
- Jian, L., Russell, C., Luhmann, J., & Skoug, R. (2006). Properties of interplanetary coronal mass ejections at one AU during 1995–2004. *Solar Physics*, 239, 393–436.
- Jiang, C., Wu, S., Feng, X., & Hu, Q. (2016). Data-driven magnetohydrodynamic modelling of a flux-emerging active region leading to solar eruption. *Nature Communications*, 7, 11522.
- Kilpua, E., Luhmann, J., Gosling, J., Li, Y., Elliott, H., Russell, C., et al. (2009). Small solar wind transients and their connection to the large-scale coronal structure. *Solar Physics*, 256, 327–344.
- Lavraud, B., Opitz, A., Gosling, J., Rouillard, A., Meziane, K., Sauvaud, J.-A., et al. (2010). Statistics of counter-streaming solar wind suprathermal electrons at solar minimum: Stereo observations. *Annals of Geophysics*, 28, 233–246.
- Lepri, S., Landi, E., & Zurbuchen, T. (2013). Solar wind heavy ions over solar cycle 23: ACE/SWICS measurements. *Astronomy Journal*, 768, 94.
- Lepri, S. T., Zurbuchen, T. H., Fisk, L. A., Richardson, I. G., Cane, H. V., & Gloeckler, G. (2001). Iron charge distribution as an identifier of interplanetary coronal mass ejections. *Journal of Geophysical Research*, 106(A12), 29,231–29,238.
- Linton, M., & Moldwin, M. (2009). A comparison of the formation and evolution of magnetic flux ropes in solar coronal mass ejections and magnetotail plasmoids. *Journal of Geophysical Research*, 114, A00B09. <https://doi.org/10.1029/2008JA013660>
- Liu, C., Deng, N., Liu, R., Ugarte-Urra, I., Wang, S., & Wang, H. (2011). A standard-to-blowout jet. *The Astrophysical Journal Letters*, 735, L18.
- Liu, Y. C.-M., Huang, J., Wang, C., Klecker, B., Galvin, A., Simunac, K., et al. (2014). A Statistical analysis of heliospheric plasma sheets, heliospheric current sheets, and sector boundaries observed in situ by STEREO. *Journal of Geophysical Research: Space Physics*, 119, 8721–8732. <https://doi.org/10.1002/2014JA019956>
- Lundquist, S. (1950). Magnetohydrostatic fields. *Arkiv för Fysik*, 2, 361–365.
- Mandrini, C. H., Pohjolainen, S., Dasso, S., Green, L., Démoulin, P., van Driel-Gesztelyi, L., et al. (2005). Interplanetary flux rope ejected from an X-ray bright point—The smallest magnetic cloud source-region ever observed. *Astronomy & Astrophysics*, 434, 725–740.
- Mao, S., He, J., Zhang, L., Yang, L., & Wang, L. (2017). Numerical study of erosion, heating, and acceleration of the magnetic cloud as impacted by fast shock. *Astronomy Journal*, 842, 109.
- McComas, D., Bame, S., Barker, P., Feldman, W., Phillips, J., Riley, P., & Griffiee, J. (1998). Solar wind electron proton alpha monitor (SWEPAM) for the advanced composition explorer. *Space Science Reviews*, 86(1–4), 563–612.
- Mistry, R., Eastwood, J. P., Phan, T. D., & Hietala, H. (2017). Statistical properties of solar wind reconnection exhausts. *Journal of Geophysical Research: Space Physics*, 122, 5895–5909. <https://doi.org/10.1002/2017JA024032>
- Moldwin, M., Ford, S., Lepping, R., Slavin, J., & Szabo, A. (2000). Small-scale magnetic flux ropes in the solar wind. *Geophysical Research Letters*, 27(1), 57–60. <https://doi.org/10.1029/1999GL010724>
- Moldwin, M., Phillips, J., Gosling, J., Scime, E., McComas, D., Bame, S., et al. (1995). Ulysses observation of a noncoronal mass ejection flux rope: Evidence of interplanetary magnetic reconnection. *Journal of Geophysical Research*, 100(A10), 19,903–19,910. <https://doi.org/10.1029/95JA01123>
- Moore, R. L., Cirtain, J. W., Sterling, A. C., & Falconer, D. A. (2010). Dichotomy of solar coronal jets: Standard jets and blowout jets. *Astronomy Journal*, 720, 757–770.
- Moore, R. L., Sterling, A. C., Falconer, D. A., & Robe, D. (2013). The cool component and the dichotomy, lateral expansion, and axial rotation of solar X-ray jets. *Astronomy Journal*, 769, 134.
- Peng, J., Liu, Y. C.-M., Huang, J., Li, H., Klecker, B., Galvin, A. B., et al. (2017). In situ analysis of heliospheric current sheet propagation. *Journal of Geophysical Research: Space Physics*, 122, 9803–9814. <https://doi.org/10.1002/2017JA024194>
- Richardson, I., & Cane, H. (2004). Identification of interplanetary coronal mass ejections at 1 AU using multiple solar wind plasma composition anomalies. *Journal of Geophysical Research*, 109, A09104. <https://doi.org/10.1029/2004JA010598>
- Rouillard, A., Savani, N., Davies, J., Lavraud, B., Forsyth, R., Morley, S., et al. (2009). A multispacecraft analysis of a small-scale transient entrained by solar wind streams. *Solar Physics*, 256, 307–326.
- Rouillard, A., Sheeley Jr., N., Cooper, T., Davies, J., Lavraud, B., Kilpua, E., et al. (2011). The solar origin of small interplanetary transients. *Astronomy Journal*, 734, 7.
- Ruffenach, A., Lavraud, B., Owens, M. J., Sauvaud, J.-A., Savani, N., Rouillard, A., et al. (2012). Multispacecraft observation of magnetic cloud erosion by magnetic reconnection during propagation. *Journal of Geophysical Research*, 117, A09101. <https://doi.org/10.1029/2012JA017624>
- Sheeley Jr., N. R., Lee, D. D.-H., Casto, K. P., Wang, Y.-M., & Rich, N. B. (2009). The structure of streamer blobs. *The Astrophysical Journal*, 694, 1471–1480. <https://doi.org/10.1088/0004-637X/694/2/1471>
- Shen, F., Wang, Y., Shen, C., & Feng, X. (2017). On the collision nature of two coronal mass ejections: A review. *Solar Physics*, 292, 104.
- Smith, E. J. (2001). The heliospheric current sheet. *Journal of Geophysical Research*, 106(A8), 15,819–15,831. <https://doi.org/10.1029/2000JA000120>
- Smith, C., L'Heureux, J., Ness, N., Acuña, M., Burlaga, L., & Scheifele, J. (1998). The ACE magnetic fields experiment. *Space Science Review*, 86, 613–632.
- Song, H., Chen, Y., Li, B., Li, L., Zhao, L., He, J., et al. (2017). The origin of solar filament plasma inferred from in situ observations of elemental abundances. *The Astrophysical Journal Letters*, 836, L11.
- Song, H., Chen, Y., Liu, K., Feng, S., & Xia, L. (2009). Quasi-periodic releases of streamer blobs and velocity variability of the slow solar wind near the Sun. *Solar Physics*, 258, 129–140.
- Song, H. Q., Zhong, Z., Chen, Y., Zhang, J., Cheng, X., Zhao, L., et al. (2016). A statistical study of the average iron charge state distributions inside magnetic clouds for solar cycle 23. *The Astrophysical Journal Supplement Series*, 224, 27. <https://doi.org/10.3847/0067-0049/224/2/27>
- Suess, S., Ko, Y.-K., Von Steiger, R., & Moore, R. (2009). Quiescent current sheets in the solar wind and origins of slow wind. *Journal of Geophysical Research*, 114, A04103. <https://doi.org/10.1029/2008JA013704>
- Tian, H., DeLuca, E., Cranmer, S., De Pontieu, B., Peter, H., Martínez-Sykora, J., et al. (2014). Prevalence of small-scale jets from the networks of the solar transition region and chromosphere. *Science*, 346, 1255711.

- Tian, H., Yao, S., Zong, Q., He, J., & Qi, Y. (2010). Signatures of magnetic reconnection at boundaries of interplanetary small-scale magnetic flux ropes. *Astronomy Journal*, 720, 454–464.
- von Steiger, R., Schwadron, N., Fisk, L., Geiss, J., Gloeckler, G., Hefti, S., et al. (2000). Composition of quasi-stationary solar wind flows from Ulysses/Solar Wind Ion Composition Spectrometer. *Journal of Geophysical Research*, 105(A12), 27,217–27,238. <https://doi.org/10.1029/1999JA000358>
- Wang, Y.-M., Sheeley, N., Socker, D., Howard, R., & Rich, N. (2000). The dynamical nature of coronal streamers. *Journal of Geophysical Research*, 105(A11), 25,133–25,142. <https://doi.org/10.1029/2000JA000149>
- Wang, Y., Zhang, Q., Liu, J., Shen, C., Shen, F., Yang, Z., et al. (2016). On the propagation of a geoeffective coronal mass ejection during 15–17 March 2015. *Journal of Geophysical Research: Space Physics*, 121, 7423–7434. <https://doi.org/10.1002/2016JA022924>
- Wang, Y., Zhou, Z., Shen, C., Liu, R., & Wang, S. (2015). Investigating plasma motion of magnetic clouds at 1 AU through a velocity-modified cylindrical force-free flux rope model. *Journal of Geophysical Research: Space Physics*, 120, 1543–1565. <https://doi.org/10.1002/2014JA020494>
- Wang, Y., Zhuang, B., Hu, Q., Liu, R., Shen, C., & Chi, Y. (2016). On the twists of interplanetary magnetic flux ropes observed at 1 AU. *Journal of Geophysical Research: Space Physics*, 121, 9316–9339. <https://doi.org/10.1002/2016JA023075>
- Yu, W., Farrugia, C., Galvin, A., Lugaz, N., Luhmann, J., Simunac, K., & Kilpua, E. (2016). Small solar wind transients at 1 AU: Stereo observations (2007–2014) and comparison with near-Earth wind results (1995–2014). *Journal of Geophysical Research: Space Physics*, 121, 5005–5024. <https://doi.org/10.1002/2016JA022642>
- Yu, W., Farrugia, C., Lugaz, N., Galvin, A., Kilpua, E., Kucharek, H., et al. (2014). A statistical analysis of properties of small transients in the solar wind 2007–2009: Stereo and wind observations. *Journal of Geophysical Research: Space Physics*, 119, 689–708. <https://doi.org/10.1002/2013JA019115>
- Zhang, J., Cheng, X., & Ding, M.-D. (2012). Observation of an evolving magnetic flux rope before and during a solar eruption. *Nature Communications*, 3, 747. <https://doi.org/10.1038/ncomms1753>
- Zhao, L., Landi, E., Lepri, S., Kocher, M., Zurbuchen, T., Fisk, L., & Raines, J. (2017). An anomalous composition in slow solar wind as a signature of magnetic reconnection in its source region. *The Astrophysical Journal Supplement Series*, 228, 4.
- Zhao, L., Zurbuchen, T., & Fisk, L. (2009). Global distribution of the solar wind during solar cycle 23: ACE observations. *Geophysical Research Letters*, 36, L14104. <https://doi.org/10.1029/2009GL039181>
- Zheng, J., & Hu, Q. (2018). Observational evidence for self-generation of small-scale magnetic flux ropes from intermittent solar wind turbulence. *The Astrophysical Journal Letters*, 852, L23.
- Zurbuchen, T. H. (2007). A new view of the coupling of the Sun and the heliosphere. *Annual Review of Astronomy and Astrophysics*, 45, 297–338.